EFFECT OF FLOW AND OPERATING PARAMETERS ON THE SPREADING OF A VISCOUS LIQUID ON A SPINNING DISC

Yuhua PAN[1*], Peter J. WITT[2], Benny KUAN[2] and Dongsheng XIE[1]

[1]CSIRO Process Science and Engineering, PO Box 312, Clayton South, Melbourne, VIC 3169, Australia
[2]CSIRO Mathematics, Informatics and Statistics, PO Box 312, Clayton South, Melbourne, VIC 3169, Australia
*Corresponding author, E-mail address: Yuhua.Pan@csiro.au

ABSTRACT

A novel dry slag granulation process based on a spinning disc is being developed by CSIRO. This process utilises centrifugal force to break up molten slag into droplets, which pass through cooling air and finally solidify into granules. In this process the sensible heat of slag is recovered as hot air. In the present work, a previously developed steady-state, two-dimensional and multiphase CFD model was applied to perform parametric numerical experiments to investigate the effects that a number of parameters have on the film thickness at the disc edge. The parameters included liquid feeding (pouring) rate, disc spinning speed, disc radius, liquid viscosity, surface tension and density. To reduce the number of simulations needed, Box and Behnken's fractional factorial design of numerical experiment was adopted. Furthermore, in order to generalise the modelling results to the atomisation of different liquids on spinning discs of different sizes, dimensional analysis was applied to develop a dimensionless correlation based on the numerical simulation data. Results of the present parametric modelling work indicate that the liquid film thickness can be significantly influenced by the liquid feeding rate, the disc radius and spinning speed, the liquid viscosity and the liquid density for a fixed liquid mass feeding rate, whereas the liquid surface tension has a negligible effect on the film thickness.

Keywords: Spinning disc, granulation, simulation, modelling, CFD, free surface flow and film thickness.

NOMENCLATURE

Alphabetic Symbols
a   constant in dimensionless equation
b   constant in dimensionless equation
c   constant in dimensionless equation
$C_{\alpha\beta}$ interphase momentum transfer term
F body force vector
F_1 first blending function in turbulence model
G   liquid feeding rate
h   liquid film thickness at disc edge
H   disc height
k turbulence kinetic energy
p pressure
P_k production rate of turbulence kinetic energy
r   volume fraction
r_n liquid feeding stream radius
R   disc radius
Re_D rotational Reynolds number

Re_n liquid feeding stream Reynolds number
u velocity vector
u_n liquid feeding stream velocity
u_θ linear velocity of disc edge
y^+ dimensionless distance

Greek Symbols
α subscript for fluid phase identity (liquid or air)
α_3 constant in turbulence model
β subscript for fluid phase identity (liquid or air)
β' constant in turbulence model
β_3 constant in turbulence model
ε dissipation rate of turbulence kinetic energy
μ dynamic viscosity
μ_t turbulent viscosity
ρ density
$\sigma_{\omega 2}$ Prandtl number for ω in transformed k-ε model
$\sigma_{\omega 3}$ Prandtl number for ω in Shear-Stress-Transport turbulence model
σ_{k3} Prandtl number for k in Shear-Stress-Transport turbulence model
ω turbulence eddy frequency
Ω disc spinning speed
Π_1 dimensionless number
Π_2 dimensionless number

INTRODUCTION

Generation of droplets, granules and powders by pouring liquid onto a rapidly spinning disc is a method known as centrifugal atomisation, which is widely applied in processes such as spray drying, scrubbing, combustion, and powder production. Advantages of centrifugal atomisation are its ability to produce droplets with a narrow size range and its applicability to liquids of both low viscosity (e.g., water) and high viscosity (e.g., organic liquids). A typical centrifugal atomisation process involves formation of a liquid film on the top surface of the disc, followed by disintegration of the film into droplets on or after leaving the edge of the disc.

Mathematical modelling of liquid flow on a spinning disc, based on analytically solving a simplified set of Navier-Stokes equations of momentum conservation and continuity, has been performed in a number of previous studies. Emslie et al. (1958) utilised a method of characteristic curves to demonstrate that a film with an initial irregular fluid distribution develops towards a uniform distribution under centrifugal effect. Zhao et al.

1

(1998) conducted experimental work to visualise the flow of liquid metal on a spinning disc and observed that for their operating conditions a hydraulic jump formed at a radial distance resulting in a sudden increase in film thickness. An analytical model was developed by Zhao et al. (1998) that described the flow of a liquid film on the spinning disc and predicted the occurrence and location of the hydraulic jump. Employing lubrication theory Myers and Charpin (2001) investigated the effect of Coriolis force on liquid film formation on a spinning disc and found that, when the flow is axisymmetric, the Coriolis force has no effect on the height of the liquid film. Deng and Ouyang (2011) used mathematical models to investigate liquid metal film instabilities and the formation of metallic powders by a spinning disc. At high rotation speeds thin discs can vibrate and this vertical motion can introduce instabilities in liquid films flowing over and leaving the disc. In their modelling work Deng and Ouyang treated the disc as a spinning Kirchhoff plate and used a combined analytical (Galerkin) and numerical (Runge–Kutta) method to calculate the vibrating modes of the disc and flow and breakup of the liquid film on leaving the vibrating plate.

However, the above-mentioned analytical and numerical modelling studies on simplified conditions generally suffer from two shortcomings: 1) neglect of turbulence effects and 2) neglect heat transfer when modelling non-isothermal flows. Turbulence is likely to play important roles in both the liquid spreading on a spinning disc and, after leaving the disc, the breakup of the film into droplets. Although heat transfer has a limited effect on liquid spreading on the disc, its effect on viscosity may significantly affect the breakup of the film and hence the formation of droplets. To overcome this deficiency, utilisation of computational fluid dynamics (CFD) in numerical studies of centrifugal atomisation has emerged in recent years. Ho and Zhao (2004) developed a CFD model to simulate the thermal development of liquid metal on a spinning disc and predicted the volume of solid skull formation on the disc. Pan et al. (2010, 2011) developed CFD models for simulating liquid slag spreading and heat transfer on a spinning disc, breakup of the slag film and formation of ligaments and droplets. Caprariis et al. (2012) applied a CFD model to simulate turbulent flows on a spinning disc reactor for nanoparticles production.

In recent years, the centrifugal atomisation method was successfully extended by CSIRO to allow processing of molten slags, a by-product of metal production. The process is called dry slag granulation (DSG) and is currently under development at CSIRO (Jahanshahi et al, 2012). This process utilises the centrifugal force imposed by the spinning disc to drive liquid slag, which is poured onto the centre of the disc, to spread into a thin film on the disc surface. On leaving the disc edge, the liquid film deforms into ligaments that eventually break up into droplets. The droplets are quenched with air to finally solidify into granules. In this process the sensible heat of slag is recovered as hot air. Figure 1 shows a photo of a semi-industrial scale DSG plant (with up to 100 kg min^{-1} liquid slag throughput). This pilot plant was constructed and is being operated at CSIRO's Clayton laboratories. Figure 2 is an image captured from the DSG plant by a high-speed video camera showing atomisation of molten slag on a spinning disc. The production of slag granules

by the DSG process has many advantages over the conventional wet (water quenching) granulation methods in that the DSG process can recover slag sensible heat (and hence reduce greenhouse gas emissions), save water and minimise air pollution (Xie and Jahanshahi, 2008).

Figure 1: The semi-industrial scale (3 m in diameter) integrated dry granulation and heat recovery pilot plant at CSIRO.
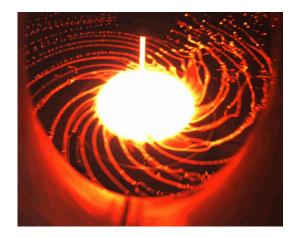

Figure 2: A typical still image from high speed video recording of the slag atomisation by a spinning disc in CSIRO's dry slag granulation process.

In the previous work, the turbulent flow and heat transfer occurring on the spinning disc in CSIRO's DSG process was modelled by developing a non-isothermal steady-state, two-dimensional and multiphase CFD model using the ANSYS CFX modelling package (Pan et al., 2010). The model predicted the thickness of the liquid slag film at the disc edge prior to its breakup into droplets.

In the present work, using the above-mentioned model, CFD simulations have been carried out to investigate effects of liquid feeding (pouring) rate, disc spinning speed, liquid viscosity, surface tension and liquid density as well as disc radius on the liquid film thickness at the disc edge. To reduce the number of numerical simulation runs, a fractional factorial design (Box and Behnken, 1960) of the numerical experiment was adopted. Furthermore, in order to generalise the modelling results to be applicable to other centrifugal atomisation systems with different viscous liquids and different disc sizes, dimensional analysis was applied to develop a dimensionless correlation based on the numerical experimental data.

MODEL FORMULATION

General Assumptions

In order to mathematically simulate the free surface flow phenomenon encountered when a liquid is poured onto a spinning disc, the following general assumptions have been made:

- Steady-state turbulent fluid flow;

- Heat transfer is neglected for a fixed viscosity, as it has a negligible influence on the liquid film thickness on the spinning disc. Further details are in previous work (Pan et al., 2010);

- A continuous liquid stream is poured along the centre axis of the disc so that rotational symmetry is assumed about the central axis of the stream and thus a two-dimensional computation domain can be applied;

- To reduce computational effort, only a part of the liquid feeding stream and a limited portion of air near the disc are included in the computation domain.

Governing Equations

In this work the liquid and air flow is modelled as a steady-state two-phase free surface flow. Location of the liquid-air interface is determined by solving a pair of phase continuity equations given in Eqn. (1).

$$\nabla \cdot \left(r_\alpha \rho_\alpha \mathbf{u}_\alpha \right) = 0 \tag{1}$$

To allow for simulation of liquid breakup in future models separate velocity fields are obtained by solving a momentum equation, generalised as Eqn. (2), for each phase.

$$\nabla \cdot \left[r_\alpha \left(\rho_\alpha \mathbf{u}_\alpha \mathbf{u}_\alpha \right) \right] = -r_\alpha \nabla p_\alpha \\ + \nabla \cdot \left[r_\alpha \left(\mu + \mu_t \right) \left(\nabla \mathbf{u}_\alpha + \left(\nabla \mathbf{u}_\alpha \right)^T \right) \right] + \mathbf{F}_\alpha + \mathbf{C}_{\alpha\beta} \tag{2}$$

where, apart from the conventional symbols (see NOMENCLATURE), $\mathbf{F}_\alpha$ is an additional momentum source accounting for surface tension at the free surface that is approximated by using the Continuum Surface Force method of Brackbill et al. (1992); and $\mathbf{C}_{\alpha\beta}$ is the interphase drag force calculated using a free surface model with the area derived from the volume fraction gradient assuming a Newtonian regime.

Shear-Stress-Transport (SST) model described by Eqns. (3) and (4) are solved to obtain the turbulent kinetic energy and turbulent eddy frequency.

$$\nabla \cdot \left(\rho \mathbf{u} k \right) = \nabla \cdot \left[\left(\mu + \frac{\mu_t}{\sigma_{k3}} \right) \nabla k \right] + P_k - \beta' \rho k \omega \tag{3}$$
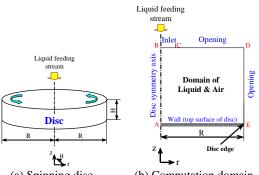
$$\nabla \cdot \left(\rho \mathbf{u} \omega \right) = \nabla \cdot \left[\left(\mu + \frac{\mu_t}{\sigma_{\omega3}} \right) \nabla \omega \right] + \left(1 - F_1 \right) 2 \rho \frac{\nabla k \nabla \omega}{\sigma_{\omega2} \omega} \\ + \alpha_3 \frac{\omega}{k} P_k - \beta_3 \rho \omega^2 \tag{4}$$

Further details of the constants and terms in the above equations are given in ANSYS (2009).

It was anticipated that there could be a wide range of Reynolds number in the fluid domain (liquid slag and air) on a spinning disc. According to Parisi et al. (2011), when the Reynolds number, defined as Re = $G/(2\pi R\mu)$, is greater than 20, the flow is turbulent. In the present work, Re ranges from 8 to 90, hence about 70% of the simulation cases were performed with Re > 20. On this basis the SST turbulence model has been used.

Disc Geometry and Computation Domain

The disc geometry is a flat cylinder of radius R and height H, as schematically illustrated in Figure 3(a). The diameter of the liquid feeding stream is set to 5, 7 or 9 mm for the liquid feeding rate of 2.5, 5 or 7.5 kg min^{-1}, respectively. Figure 3(b) shows the two-dimensional computation domain covering half the disc top surface and a region enclosing parts of liquid and air above the disc top surface. (The disc body is excluded from the computation domain.) In the radial direction, due to rotational symmetry, the computation domain only extends from the disc axis to the disc edge.

| (a) Spinning disc | (b) Computation domain |

Figure 3: Schematic diagrams of three-dimensional disc geometry and two-dimensional computational domain.

In order to resolve the liquid layer and free surface, the mesh element size should be sufficiently small in the vicinity above the disc's top surface. According to preliminary simulations with different mesh element sizes, an element size smaller than 0.25 mm was found appropriate and thus employed in all the subsequent simulations. In the vicinity of the disc surface, a small element size normal to the wall was set. The dimensionless distance from the disc surface to the first nodal point in the fluid domain, y^+, was controlled to be around 0.1. Using such a y^+ with the SST turbulence model and near wall treatment in CFX, results in the flow being numerically integrated up to the solid surface and that turbulent log layer wall functions was not used.

Boundary Conditions

In the computation domain shown in Figure 3(b), the boundaries are named and labelled in an alphabetical order, for which the specified conditions are given in Table 1.

Table 1: Boundary conditions.

Boundary	Type	Condition
AB	Axis of symmetry	Zero fluxes
BC	Inlet	Liquid mass flowrate = Feeding rate (kg s^{-1})
CD & DE	Opening	External relative pressure = 0 (Pa)
EA	Wall	No slip
		Angular velocity = Spinning speed (rad s^{-1})

3

Material Properties

Table 2 gives the material physical properties used as a benchmark condition in the present modelling work. In the parametric numerical experiment, the value of each property of the liquid phase is varied by ± 50% from the benchmark value of liquid slag.

Table 2: Benchmark material physical properties.

Material	Density (kg m^{-3})	Dynamic viscosity (Pa·s)	Surface tension (N m^{-1})
Liquid slag[1]	2590[a]	0.7[b]	0.478[a]
Air (at 25 °C)[2]	1.185	1.831×10^{-5}	-

[1] a: Inaba et al. (2004), b: Purwanto et al. (2005).
[2] ANSYS (2009).

Solution Method

The governing equations expressed by Eqns. (1) through (4) together with the boundary conditions given in Table 1 were solved numerically using the commercial CFD modelling package ANSYS CFX 12 (ANSYS, 2009).

Model Validity and Limitation

The CFD model described above is an isothermal version of the previously developed non-isothermal CFD model that was already validated against experimental measurements on the thickness of solid slag crusts formed on the disc top surface (Pan et al., 2010). Therefore, we presume that the validity of the previous model would be inherent in the present one.

It should be mentioned that the two-dimensional model has a strict limitation in predicting radial flow features, such as three-dimensional wave formations that have been noted by a number of researchers. That is, the liquid film does not rupture within the disc radius. Therefore, this limitation also imposes an upper bound on the size of the disc that can be modelled depending on liquid feeding rate and spinning speed. For example, the model is only valid for a combination of high feeding rate, low spinning speed and small diameter discs.

DIMENSIONAL ANALYSIS

In order to analyse results from the multi-parameter modelling study, it is useful to identify dimensionless ratios that are key to characterising the spreading behaviour of different liquids on spinning discs of different sizes and under different operating conditions. In this way, a dimensionless correlation bridging the influencing parameters and the target parameter can be obtained via which the modelling results could be conveniently applied to other systems of different scales.

In the present work, the following parameters are considered as the influencing parameters:
- Liquid feeding rate (G)
- Disc spinning speed (Ω)
- Disc radius (R)
- Liquid viscosity (μ)
- Liquid density (ρ)

The liquid film thickness (h) at the disc edge is considered as the target parameter as we anticipate that this parameter would heavily affect the droplet formation and size distribution. As will be seen in a later section, model simulations indicate that liquid surface tension has a negligible effect on the liquid film thickness and thus is excluded in the parametric numerical experiment.

The relationship between above-mentioned influencing and target parameters can be described by a general function as

$$h = f(G, \Omega, R, \mu, \rho) \qquad (5)$$

By means of dimensional analysis, Eqn. (5) can be transformed into the following dimensionless form:

$$\frac{h}{R} = g\left(\frac{\rho \Omega R^2}{\mu}, \frac{\mu R}{G}\right) \qquad (6)$$

Interpretations on the derived independent dimensionless numbers in Eqn. (6) are as follows:

$$\Pi_1 = \frac{\rho \Omega R^2}{\mu} = \frac{\rho u_\theta R}{\mu} = \text{Re}_D \qquad (7)$$

$$\Pi_2 = \frac{\mu R}{G} = \frac{R}{\frac{\rho u_n r_n}{\mu} \cdot \pi r_n} = \frac{1}{\pi} \cdot \frac{R/r_n}{\text{Re}_n} \qquad (8)$$

where $u_\theta = \Omega R$ is linear velocity of the disc edge (m s^{-1}); Re_D is the Reynolds number at the disc edge (called rotational Reynolds number); u_n and r_n are liquid feeding stream velocity (m s^{-1}) and radius (m), respectively; and Re_n is liquid feeding stream Reynolds number. Thus, Eqn. (6) implies that the dimensionless liquid film thickness (h/R) is a function of the rotational Reynolds number and the feeding stream Reynolds number as well as the ratio between the disc and the feeding stream radii. It may be anticipated here that h/R will decrease with the increases of Re_D and R/r_n but increase with the increase of Re_n.

The detail (empirical) form of Eqn. (6) is normally cast, using power law functions, into

$$\frac{h}{R} = a\left(\frac{\rho \Omega R^2}{\mu}\right)^b \left(\frac{\mu R}{G}\right)^c \qquad (9)$$

where a, b, and c are constants that should be determined from the results of (numerical) experiments.

Within the data range investigated in the present work, Eqn. (9) can be used for scaling up the atomisation process for different liquids and disc sizes. Nevertheless, it is crucial to determine the constants a, b and c from well-representative experimental results by performing, ideally, a full factorial experiment. However, considering that there are five factors (parameters), i.e., G, Ω, R, μ and ρ, if each with a three variation levels, a full factorial experiment would require $3^5 = 243$ runs, which is impractical. Therefore, in this work, we adopted a fractional factorial experimental design of Box and Behnken (1960) to perform the parametric numerical experiment so as to determine the constants a, b and c in Eqn. (9).

FRACTIONAL FACTORIAL DESIGN OF PARAMETRIC EXPERIMENTS

Box and Behnken (1960) proposed a useful method for designing incomplete three-level experiments, which is widely used for investigating nonlinear (quadratic) effects of multi-parameters. By using their method, a fractional factorial design of experiment on five parameters each with three levels (3^5 experimental design for short) is listed in Table 3. The level of each parameter is set by varying its value by $\pm 25\%$, $\pm 33.3\%$ or $\pm 50\%$ from the median (benchmark) level.

As seen from Table 3, the total number of required numerical runs is reduced to an affordable 41. Therefore, according to the conditions specified in Table 3, 41 numerical simulations were carried out and the predicted liquid film thickness values were included in the last column of Table 3.

Taking the logarithm of Eqn. (9) yields

$$\ln\left(\frac{h}{R}\right) = \ln(a) + b\ln\left(\frac{\rho \Omega R^2}{\mu}\right) + c\ln\left(\frac{\mu R}{G}\right) \quad (10)$$

Using the data in Table 3 and performing multiple linear regression analysis on Eqn. (10) yield a = 0.479, b = -0.612 and c = -0.336. Thus, the detail form of Eqn. (9) is obtained as

$$\frac{h}{R} = 0.479\left(\frac{\rho \Omega R^2}{\mu}\right)^{-0.612}\left(\frac{\mu R}{G}\right)^{-0.336} \quad (11)$$

Figure 4 shows a parity comparison between the left hand side and right hand side terms in Eqn. (11) using the data given in Table 3. This figure indicates that all data are reasonably distributed along the diagonal line (Regression R-squared = 0.92), demonstrating the validity of Eqn. (9).

Eqn. (11) can be transformed into an explicit dimensional form as

$$h = 0.479\frac{G^{0.336}\mu^{0.275}}{\Omega^{0.612}R^{0.56}\rho^{0.612}} \quad (12)$$

which, because of the magnitudes of the exponents, confirms that the effects of all the five parameters are indeed rather significant. Eqn. (12) further indicates that the liquid film thickness increases with increasing liquid feeding rate and viscosity but decreases with increasing disc spinning speed, disc radius and liquid density.

Table 3: 3^5 fractional factorial design of numerical experiment.

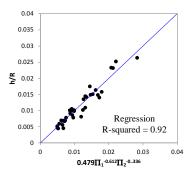| Liquid feeding rate G (kg min⁻¹)	Disc spinning speed Ω (RPM)	Disc radius R (mm)	Liquid viscosity μ (Pa s)	Liquid density ρ (kg m⁻³)	Liquid film thickness h (mm)
2.5	1500	37.5	0.7	2590	0.383
7.5	1500	37.5	0.7	2590	0.535
2.5	2500	37.5	0.7	2590	0.261
7.5	2500	37.5	0.7	2590	0.372
5	2000	25	0.35	2590	0.379
5	2000	50	0.35	2590	0.227
5	2000	25	1.05	2590	0.584
5	2000	50	1.05	2590	0.339
5	1500	37.5	0.7	1295	0.595
5	2500	37.5	0.7	1295	0.412
5	1500	37.5	0.7	3885	0.398
5	2500	37.5	0.7	3885	0.173
2.5	2000	25	0.7	2590	0.374
7.5	2000	25	0.7	2590	0.581
2.5	2000	50	0.7	2590	0.237
7.5	2000	50	0.7	2590	0.347
5	2000	37.5	0.35	1295	0.385
5	2000	37.5	1.05	1295	0.559
5	2000	37.5	0.35	3885	0.259
5	2000	37.5	1.05	3885	0.381
5	1500	25	0.7	2590	0.632
5	2500	25	0.7	2590	0.411
5	1500	50	0.7	2590	0.394
5	2500	50	0.7	2590	0.300
2.5	2000	37.5	0.35	2590	0.212
7.5	2000	37.5	0.35	2590	0.326
2.5	2000	37.5	1.05	2590	0.346
7.5	2000	37.5	1.05	2590	0.51
5	2000	25	0.7	1295	0.66
5	2000	50	0.7	1295	0.395
5	2000	25	0.7	3885	0.439
5	2000	50	0.7	3885	0.261
2.5	2000	37.5	0.7	1295	0.307
7.5	2000	37.5	0.7	1295	0.529
2.5	2000	37.5	0.7	3885	0.264
7.5	2000	37.5	0.7	3885	0.382
5	1500	37.5	0.35	2590	0.384
5	2500	37.5	0.35	2590	0.263
5	1500	37.5	1.05	2590	0.545
5	2500	37.5	1.05	2590	0.379
5	2000	37.5	0.7	2590	0.380
5	2000	37.5	0.7	2590	0.380
5	2000	37.5	0.7	2590	0.380
5	2000	37.5	0.7	2590	0.380
5	2000	37.5	0.7	2590	0.380
5	2000	37.5	0.7	2590	0.380

Figure 4: Plot of h/R with $0.479\Pi_1^{-0.612}\Pi_2^{-0.336}$ using the data given in Table 3

5

RESULTS AND DISCUSSION

Prediction of Free Surface Profile and Flow Field

One of the important objectives of the present CFD modelling work is to predict the liquid free surface profile and especially the film thickness at the disc edge. As an example, Figure 5 shows the predicted (a) molten slag free surface profile and (b) velocity field. The free surface profile is indicated by the border between the red colour region (liquid) and the blue colour region (air). The predicted velocity field depicts a strong downward flow of the feeding stream and high radial velocities liquid and air in the vicinity of the free surface. Away from the liquid film, the air flow decays rapidly and so is the liquid flow close to the disc top surface due to wall friction.

(a) Free surface profile

(b) Velocity field

Figure 5: Predicted (a) liquid slag free surface profile and (b) velocity field for feeding rate: 5 kg min^{-1}, spinning speed: 2000 RPM, disc radius: 25 mm.

Influence of Parameters on Liquid Film Thickness

Figures 6 to 10 show the effect that changes in various parameters have on the liquid film thickness calculated using Eqn. (12) and in comparison with data of numerical experiments under the same conditions. These figures indicate a good agreement between Eqn. (12) and the individual simulation results, demonstrating that the dimensionless correlation Eqn. (11) is capable of quite accurately representing the numerical experimental results. This further implies that the general dimensionless correlation Eqn. (9) is potentially applicable for predicting the film thickness of different liquids spreading on spinning discs of different sizes.

Influence of liquid feeding rate

From the present modelling investigation, it was found that the liquid feeding rate has a major influence on the liquid film thickness, as shown in Figure 6, which indicates that an increase (or a decrease) of the feeding rate by 50% from its benchmark value (5 kg min^{-1}) results in a 13% increase (or 22% decrease) of the liquid film thickness.
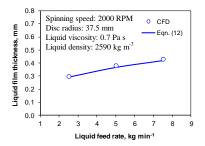

Figure 6: Influence of feeding rate on film thickness.

Influence of disc spinning speed

The most obvious influence of spinning speed is found on the liquid film thickness, as depicted by Figure 7. We can see from this figure that an increase (or a decrease) of the spinning speed by 25% from its benchmark value (2000 RPM) results in a 17% decrease (or 23% increase) of the liquid film thickness.
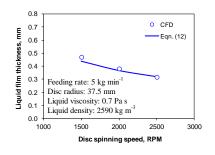

Figure 7: Influence of spinning speed on film thickness.

Influence of disc radius

Figure 8 depicts the influence of disc radius on film thickness. For a given feeding rate and spinning speed, liquid is spread more thinly on a larger disc and vice versa. For instance, an increase (or a decrease) of the disc radius by about 33% from its benchmark value (37.5 mm) results in a 22% decrease (or 36% increase) of the liquid film thickness.
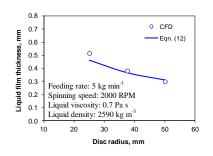

Figure 8: Influence of disc radius on film thickness.

Influence of liquid viscosity

The influence of liquid viscosity can be seen from Figure 9, which indicates that an increase (or a decrease) of the viscosity by 50% from its benchmark value (0.7 Pa s)

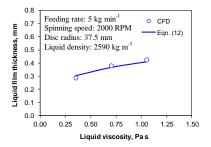results in a 12% increase (or 24% decrease) of the liquid film thickness.

Figure 9: Influence of viscosity on film thickness.

Influence of liquid density

Figure 10 shows that a change in liquid density by plus (or minus) 50% from its benchmark value (2590 kg m^{-3}) leads to a decrease by 27% (or an increase by 62%) in the film thickness. This is primarily because, for a given mass feeding rate, a denser liquid will have a smaller volumetric flowrate resulting in a thinner liquid film and vice versa.
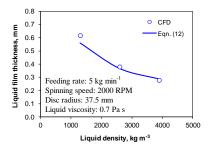

Figure 10: Influence of density on film thickness.

Influence of liquid surface tension

Finally, the effect of liquid surface tension was also examined prior to performing the numerical experiment. As demonstrated by Figure 11, surface tension has a negligible influence on film thickness. This is because the free surface of liquid spreading on the spinning disc has very little curvature except where the liquid stream first contacts the disc. As liquid approaches the disc edge the curvature is negligible (c.f., Figure 5), leading to a negligible surface tension force acting on the free surface. Nevertheless, it can be anticipated that surface tension will play a significant role in liquid breakup and droplet formation when the liquid leaves the disc, as was demonstrated in our previous CFD modelling results (Pan et al., 2011).
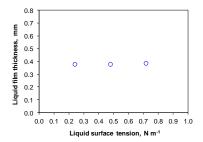

Figure 11: Influence of surface tension on film thickness. (Feeding rate: 5 kg min^{-1}, Spinning speed: 2000 RPM, Disc radius: 37.5 mm, Viscosity: 0.7 Pa s, Density: 2590 kg m^{-3})

CONCLUSIONS

A fractional factorial parametric numerical experiment combined with dimensional analysis was performed using a steady-state two-dimensional multiphase CFD model to simulate a viscous liquid spreading on a flat spinning disc to investigate the influences of multi-parameters on the liquid film thickness at the disc edge prior to its breakup into droplets. From the modelling results the following conclusions can be drawn:

- Liquid feeding rate, disc spinning speed, disc radius, and liquid viscosity and density all have significant influences on the liquid film thickness at the disc edge.
- An increase (or a decrease) by 50% of liquid feeding rate, liquid viscosity and density from their benchmark values (5 kg min^{-1}, 0.7 Pas s and 2590 kg m^{-3}) results in a variation in the liquid film thickness by +13% (or -22%), +12% (or -24%) and -27% (or +62%), respectively.
- An increase (or a decrease) by 25% of disc spinning speed from its benchmark value (2000 RPM) leads to 17% decrease (or 23% increase) in the liquid film thickness.
- An increase (or a decrease) by about 33% of disc radius from its benchmark value (37.5 mm) yields 22% decrease (or 36% increase) in the liquid film thickness.
- Liquid surface tension has a negligible effect on the liquid film thickness.
- Within the parameter ranges investigated in the present work, a dimensionless correlation was developed that can be used to predict the film thickness of different liquids spreading on flat discs of larger or reduced sizes. In addition, the general dimensionless correlation developed in this work could potentially be applicable to a wider variety of atomisation systems using flat spinning discs.

ACKNOWLOGMENT

REFERENCES

ANSYS Inc., 2009, ANSYS CFX User Manual, Release 12.0.

BRACKBILL, J.U.; KOTHE, D.B. and ZEMACH, C., (1992), "A continuum method for modelling surface tension", *Journal of Computational Physics*, **100**, 335-354.

BOX, G.E.P. and BEHNKEN, D.W., (1960), "Some new three level designs for the study of quantitative variables", *Technometrics*, **2**, No. 4, 455-475.

CAPRARIIS, B. de; RITA, M. Di; STOLLER, M.; VERDONE, N. and CHIANESE, A., (2012), "Reaction-precipitation by a spinning disc reactor: influence of hydrodynamics on nanoparticles production", *Chemical Engineering Science*, **76**, 73-80.

DENG, H. and OUYANG, H., (2011), "Vibration of spinning discs and powder formation in centrifugal atomization", *Proceedings of the Royal Society A*, **467**, 361-380.

EMSLIE, A.G.; BONNER, F.T. and PECK, L.G., (1958), "Flow of a viscous liquid on a rotating disk", *Journal of Applied Physics*, **29**, No. 5, 858-862.

HALADA, K.; SUGA, H. and MURAMATSU, Y., (1990), "Atomizing parameters for centrifugal atomization of metal", *Proceedings of the International Conference of Powder Metallurgy: PM into the 1990's*, 2-6 July 1990, London, U.K., 193-199.

HO, K.H. and ZHAO, Y.Y., (2004), "Modelling thermal development of liquid metal flow on rotating disc in centrifugal atomisation", *Materials Science and Engineering*, **A365**, 336-340.

INABA, S.; KIMURA, Y.; SHIBATA, H. and OHTA, H., (2004), "Measurement of physical properties of slag formed around the raceway in the working blast furnace", *ISIJ International*, **44**, No. 12, 2120-2126.

JAHANSHAHI, S.; XIE, D.; PAN, Y.; RIDGEWAY, P. and MATHIESON, J., (2011), "Dry slag granulation with integrated heat recovery", *METEC InSteelCon® 2011 Conference Proceedings*, Düsseldorf, Germany, 27 June – 2 July 2011, Session 11, 1-7.

LIU, Y-Z.; MINAGAWA, K. and HALADA, K.K., (2007), "Melt film formation and disintegration during novel atomization process", *Transactions of Nonferrous Metals Society of China*, **17**, 1276-1281.

MATSUMOTO, S.; SAITO, K. and TAKASHIMA, Y., (1974), "Phenomenal transition of liquid atomization from disk", *Journal of Chemical Engineering of Japan*, **7**, No. 1, 13-19.

MYERS, T.G. and CHARPIN, J.P.F., (2001), "The effect of the Coriolis force on axisymmetric rotating thin film flows", *International Journal of Non-Linear Mechanics*, **36**, 629-635.

PAN, Y.; WITT, P.J. and XIE, D., (2010), "CFD simulation of free surface flow and heat transfer of liquid slag on a spinning disc for a novel dry slag granulation process", *Progress in Computational Fluid Dynamics*, **10**, Nos. 5-6, 292-299.

PAN, Y.; WITT, P.J.; KUAN, B. and XIE, D., (2011), "CFD simulation of slag droplet formation by a spinning disc in dry slag granulation processes", *8th International Conference on CFD in Oil & Gas, Metallurgical and Process Industries*, 21-23 June 2011, Trondheim, Norway.

PARISI, M.; STOLLER, M. and CHIANESE, A. (2011), "Production of Nanoparticles of Hydroxyapatite by Using a Rotating Disk Reactor", *The tenth International Conference on Chemical & Process Engineering (ICheaP-10)*, 8-11 May 2011, Florence, Italy.

PURWANTO, H.; MIZUOCHI T. and AKIYAMA T., (2005), "Prediction of granulated slag properties produced from spinning disk atomizer by mathematical model", *Materials Transactions*, **46**, No. 6, 1324-1330.

XIE, D. and JAHANSHAHI, S., (2008), "Waste heat recovery from molten slags", *International Congress on Steel 2008 (ICS2008)*, 6-8 October 2008, Gifu, Japan.

ZHAO, Y.Y.; JACOBS, M.H. and DOWSON, A.L., (1998), "Liquid flow on a rotating disk prior to centrifugal atomization and spray deposition", *Metallurgical and Materials Transactions B*, **29B**, 1357-1369.